



Cite this: *Phys. Chem. Chem. Phys.*,
2020, **22**, 21131

Net negative contributions of free electrons to the thermal conductivity of NbSe₃ nanowires†

Zhiliang Pan, ^{#a} Lin Yang, ^{#a} Yi Tao, ^{ab} Yanglin Zhu, ^c Ya-Qiong Xu, ^{de} Zhiqiang Mao^c and Deyu Li ^{*a}

Understanding transport mechanisms of electrons and phonons, two major energy carriers in solids, are crucial for various engineering applications. It is widely believed that more free electrons in a material should correspond to a higher thermal conductivity; however, free electrons also scatter phonons to lower the lattice thermal conductivity. The net contribution of free electrons has been rarely studied because the effects of electron–phonon (e–ph) interactions on lattice thermal conductivity have not been well investigated. Here an experimental study of e–ph scattering in quasi-one-dimensional NbSe₃ nanowires is reported, taking advantage of the spontaneous free carrier concentration change during charge density wave (CDW) phase transition. Contrary to the common wisdom that more free electrons would lead to a higher thermal conductivity, results show that during the depinning process of the condensed electrons, while the released electrons enhance the electronic thermal conductivity, the overall thermal conductivity decreases due to the escalated e–ph scattering. This study discloses how competing effects of free electrons result in unexpected trends and provides solid experimental data to dissect the contribution of e–ph scattering on lattice thermal conductivity. Lastly, an active thermal switch design is demonstrated based on tuning electron concentration through electric field.

Received 29th June 2020,
Accepted 14th September 2020

DOI: 10.1039/d0cp03484c

rsc.li/pccp

Introduction

Free electrons and phonons are two major energy carriers in solids that are responsible for thermal transport in metallic and non-metallic materials, respectively. It is generally expected that a higher free electron concentration could help to enhance thermal conductivity, as shown in the well-known plot illustrating thermoelectric properties as a function of the carrier concentration.¹ However, free electrons could also scatter phonons, which could lead to a reduced lattice thermal conductivity. As such, the net contribution of free electrons on materials thermal conductivity needs more careful examination.

While the positive contribution of free electrons to thermal transport can usually be evaluated using the Wiedemann–Franz law as a good approximation, the negative contribution through electron–phonon (e–ph) scattering has received relatively less attention and in fact, is often neglected in modeling lattice thermal conductivity of semiconductors. In contrast, extensive studies of other phonon scattering mechanisms, including phonon–phonon,^{2–5} phonon-boundary,^{6–9} and phonon-defects,^{10,11} have been carried out intensively in the past two decades in the efforts of understanding thermal transport through nanostructures and interfaces for better thermal management of electronic devices and construction of novel energy converters. This is partly due to the lack of experimental data clearly demonstrating the effects of e–ph scattering on phonon transport because in semiconductors, altering free electron concentrations through doping inevitably introduces defect scattering and it is difficult to distinguish the effects of e–ph scattering from those of defects.

Recently, using first principles calculations, it has been shown that e–ph scattering could have significant effects on the lattice thermal conductivity of heavily doped Si, metals, and SiGe alloys. For example, Liao *et al.*¹² reported that e–ph scattering could lead to up to ~45% reduction in the lattice thermal conductivity of heavily-doped silicon, which was overlooked in most previous studies. In addition, the influence of e–ph scattering on the lattice thermal conductivity of various metals has been examined by Wang *et al.*,¹³ as well as Jain and

^a Department of Mechanical Engineering, Vanderbilt University, Nashville, TN 37235, USA. E-mail: deyu.li@vanderbilt.edu

^b School of Mechanical Engineering and Jiangsu Key Laboratory for Design and Manufacture of Micro-Nano Biomedical Instruments, Southeast University, Nanjing, 210096, P. R. China

^c Department of Physics, Pennsylvania State University, University Park, PA 16802, USA

^d Department of Electrical Engineering and Computer Science, Vanderbilt University, Nashville, TN 37235, USA

^e Department of Physics and Astronomy, Vanderbilt University, Nashville, TN 37235, USA

† Electronic supplementary information (ESI) available. See DOI: 10.1039/d0cp03484c

‡ These authors contribute to the paper equally.

McGaughey;¹⁴ and both studies suggested significant impacts of e-ph scattering, especially in the lower temperature regime. The most remarkable result was reported by Xu *et al.*,¹⁵ which suggested a 60% reduction in lattice thermal conductivity of SiGe upon introducing the e-ph interactions.

Experimental attempts to clarify the effects of e-ph scattering on lattice thermal conductivity include some early measurements on heavily doped semiconductors;¹⁶ however, the complex phonon scattering process renders the analysis to be only qualitative. More recently, Liao *et al.*,¹⁷ measured the scattering rate between 250 GHz phonons and dynamically pumped electron-hole pairs in Si membrane to quantify the influence of e-ph scattering. In addition, we reported more direct data showing distinct signatures of e-ph scattering in the lattice thermal conductivity of NbSe₃ nanowires as free electrons condensed due to charge density wave (CDW) phase transitions. In this paper, through reactivating the condensed electrons in NbSe₃ nanowires in the temperature range between 41 and 59 K by electric field induced depinning, we further demonstrate that free electrons do not always contribute positively to thermal conductivity, which provides insights into the competing roles of free electrons in terms of thermal transport.

Experimental approach

NbSe₃ belongs to a class of quasi-one-dimensional (quasi-1D) crystals composed of covalently-bonded molecular chains assembled together *via* weak van der Waals (vdW) interactions, as schematically shown in Fig. 1a. The aligned molecular chains can be clearly seen in the high-resolution transmission electron microscopy (HRTEM) micrograph in Fig. 1b; and the high-quality crystalline structure is verified by the selected area electron diffraction (SAD) pattern. The unique crystal structure renders interesting properties such as two CDW phase transitions, which correspond to spontaneous escalation of the electrical resistance as temperature drops to 145 K and 59 K, respectively, due to condensation of free electrons. This provides an ideal platform to study the effects of e-ph scattering on thermal transport as the spontaneous change of free electron concentration does not involve any alteration of the doping level, as discussed in our recent publication on the distinct signatures in the lattice thermal conductivity of NbSe₃ nanowires¹⁸ and more recently, Liu's work on 1T-TaS₂ nanowires.¹⁹

One interesting trait of CDW phase transitions is that the condensed electrons can be reactivated readily by an applied electric field.^{20,21} As CDW develops, the condensed free electrons are pinned to defects and surfaces, as a result of Fermi surface nesting.²² However, a rather small electric field can depin the condensed electrons to become free electrons again, which would contribute to both electrical and thermal transport. To examine the net effect of these electrons on thermal transport, we measure the thermal conductivity of NbSe₃ nanowires without and with depinning the condensed electrons through modifying a well-established experimental scheme.^{23,24}

NbSe₃ nanowires were prepared *via* liquid phase ultrasonic exfoliation from bulk crystals, which leads to small wires of

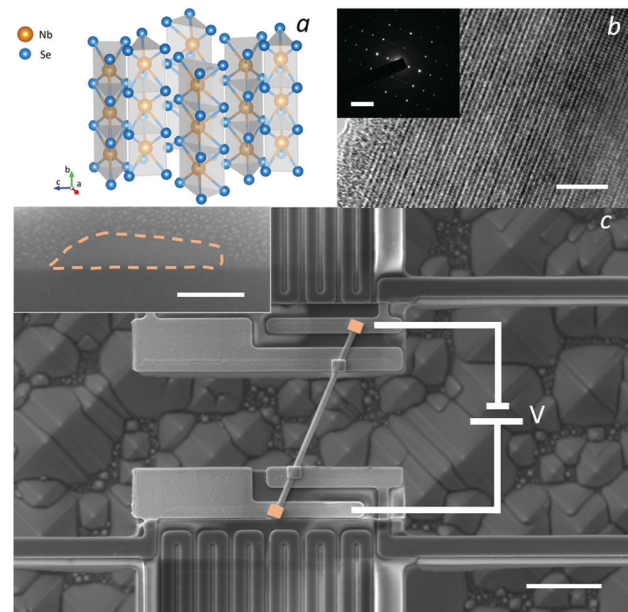


Fig. 1 Crystal structure of NbSe₃ and suspended microdevice for thermal and electrical measurements. (a) A schematic diagram illustrating the crystalline structure of NbSe₃. (b) HRTEM image of a NbSe₃ nanowire showing the well-aligned molecular chains. Inset: The selected area electron diffraction (SAD) pattern. The well defined pattern indicates the single crystalline structure. Scale bar: 5 nm (main panel); 5 nm (inset). (c) An SEM image of the measurement device with a NbSe₃ nanowire placed in between the two membranes. Inset: Cross section of the measured nanowire. Scale bar: 5 μm (main panel); 100 nm (inset).

irregular cross-sections with aligned molecular chains.²⁵ The nanowires were then drop-casted onto a piece of polydimethylsiloxane (PDMS) and transferred to a measurement device and aligned between two side-by-side suspended membranes with integrated platinum resistance heaters/thermometers and electrodes, as shown in Fig. 1c. Electron beam induced deposition (EBID) was done using a dual-beam focused ion beam (FIB, FEI Helios NanoLab G3 CX) to locally deposit Pt/C mixture at the wire-electrode contacts to minimize the contact electrical and thermal resistance. The cross-section of the wire (inset of Fig. 1c) was obtained through direct observation using scanning electron microscopy (SEM) after it was cut open with the FIB following a procedure that we have reported before.²⁵ We calculate the hydraulic diameter (D_h), 4 times the reciprocal of the surface-area-to-volume ratio (S/V), as the characteristic size of the nanowire for transport properties as it better represents the surface effects.²⁶

Results and discussion

Without depinning, the measured electrical resistance and thermal conductivity (including the total, electronic and lattice thermal conductivities, κ_t , κ_e , and κ_{ph} , respectively) for a 135 nm diameter wire are shown in Fig. 2a, which agree well with our previous data.¹⁸ Here κ_e is calculated using the Wiedemann–Franz law with the Lorenz number taking as the

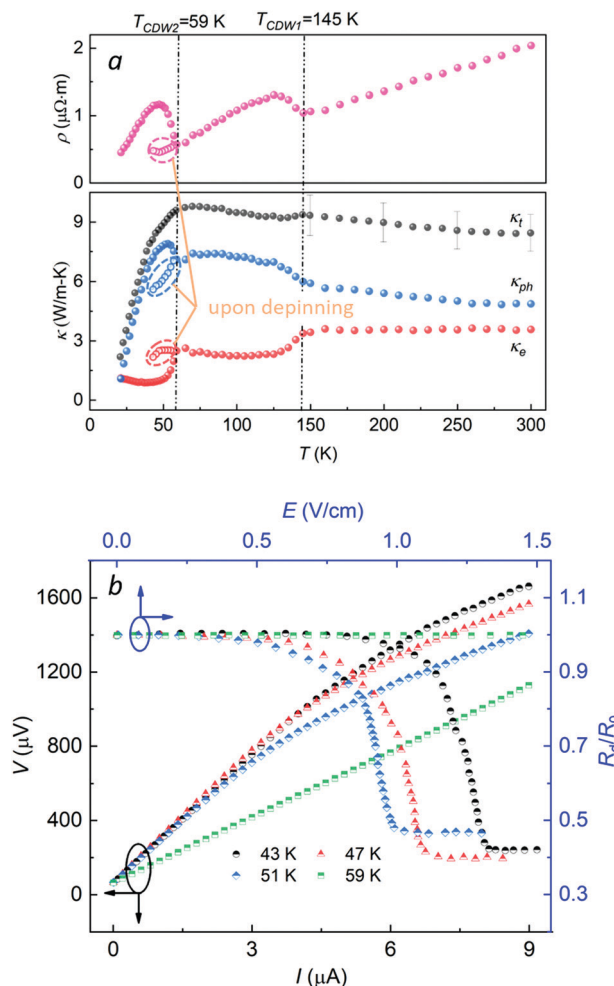


Fig. 2 Depinning effect in NbSe_3 nanowires. (a) Measured pinning and depinning data for a sample with $D_h = 135 \text{ nm}$. The open dots show the data upon depinning. (b) Left-Bottom axis: I - V curves of a NbSe_3 nanowire ($D_h = 135 \text{ nm}$) at different temperatures during the depinning test. Right-Up axis: Resistance with respect to the applied electric field upon depinning normalized by the resistance when the electric field is zero for the same wire.

Sommerfeld value, which is a very good approximation for NbSe_3 as we showed earlier.¹⁸ The obtained data match our previous results very well with two CDWs occurring at 145 K and 59 K, respectively, and the distinct signatures in κ_{ph} . To explore the depinning effects, we first examined the electrical resistance under different applied electric fields. Fig. 2b shows the measured I - V curves of the same NbSe_3 nanowire at 4 different temperatures in the 2nd CDW regime occurring at 59 K. Note that the 2nd CDW phase transition is selected due to the lower threshold of the electric field required for CDW depinning compared with the first CDW transition.²⁷ For temperatures lower than 59 K, the I - V curve deviates from a linear profile as the applied electric field is beyond a critical value, indicating that the nanowire resistance drops due to depinning of condensed electrons, which is consistent with previous reports.^{20,21,28–30} As the electric field further increases beyond certain level, however, the I - V curve becomes linear

again as most of the condensed electrons are depinned, and the resistance under depinning electric field, R_d , does not change further with the electric field, as shown in Fig. 2b. In our measurements, the maximum temperature rise of the nanowire due to Joule heating from the depinning electric field is kept to be less than 6 K to minimize the temperature deviation from the set baseline temperature.

This depinning effect leads to a nanowire resistance change, and we define a resistance ratio as $r = R_0/R_d$, where R_0 and R_d denote the electrical resistance without and with the depinning electric field, respectively. Given that the nanowire dimension remains the same during the depinning process, the resistance ratio can be written as $r = \sigma_d/\sigma_0 = (n_d e \mu)/(n_0 e \mu)$. Here σ_d and σ_0 are the electrical conductivity; n_d and n_0 the corresponding carrier concentration under the depinned and pinned conditions. e is the elementary charge; and μ the electron mobility. Bardekn *et al.*³¹ pointed out that the electron mobility is related to elastic properties of the material; and it has been shown that the measured Young's modulus of NbSe_3 remains nearly the same ($\Delta E/E_0 < 0.01\%$) with the application of the electric field.³² Moreover, Ong *et al.*, directly measured the electron mobility of NbSe_3 near the 2nd CDW phase transition temperature, which shows no carrier-concentration-dependence as CDW develops, confirming the negligible effects of the condensed electrons on charge carrier mobility.³³ Therefore, it is reasonable to assume that μ remains the same at a given temperature without and with the depinning electric field. In this case, $r = n_d/n_0$, that is, the resistance ratio can be regarded as the ratio of free carrier concentrations under depinned and pinned conditions.

Fig. 3a plots the extracted r for three different diameter wires, which indicates that as the nanowire size increases from 94 nm to 135 nm, r becomes larger. This means for thicker nanowires, a relatively larger portion of electrons can be released by the depinning electric field. Two main CDW pinning mechanisms need to be considered in NbSe_3 nanowires: surface and impurity pinning, and for nanowires with smaller diameters, a relatively larger portion of electrons are pinned at surfaces due to the larger surface-area-to-volume ratio. Meanwhile, it has been suggested that electrons pinned by the surface are more difficult to be released compared to those pinned by impurities.^{34–40} As such, the relatively low electric field applied in our measurements ($1.1\text{--}1.4 \text{ V cm}^{-1}$), which is not strong enough to fully active surface-pinned²⁷ electrons renders a lower r for smaller hydraulic diameter wires as a result of their larger surface-area-to-volume ratio.

The enhancement of the free electron concentration upon depinning corresponds to an increase of the electronic thermal conductivity (κ_e), which is also shown in Fig. 3a. The most significant enhancement is observed for the largest wire with $D_h = 135 \text{ nm}$, which demonstrates an r of ~ 2.6 , leading to a $\sim 160\%$ increment in κ_e . This change contributes positively to the nanowire thermal conductivity.

The release of more free electrons, however, also leads to enhanced e-ph scattering, which poses resistance to phonon transport, and contributes negatively to the wire thermal conductivity. Indeed, the measured κ_t of the nanowires does

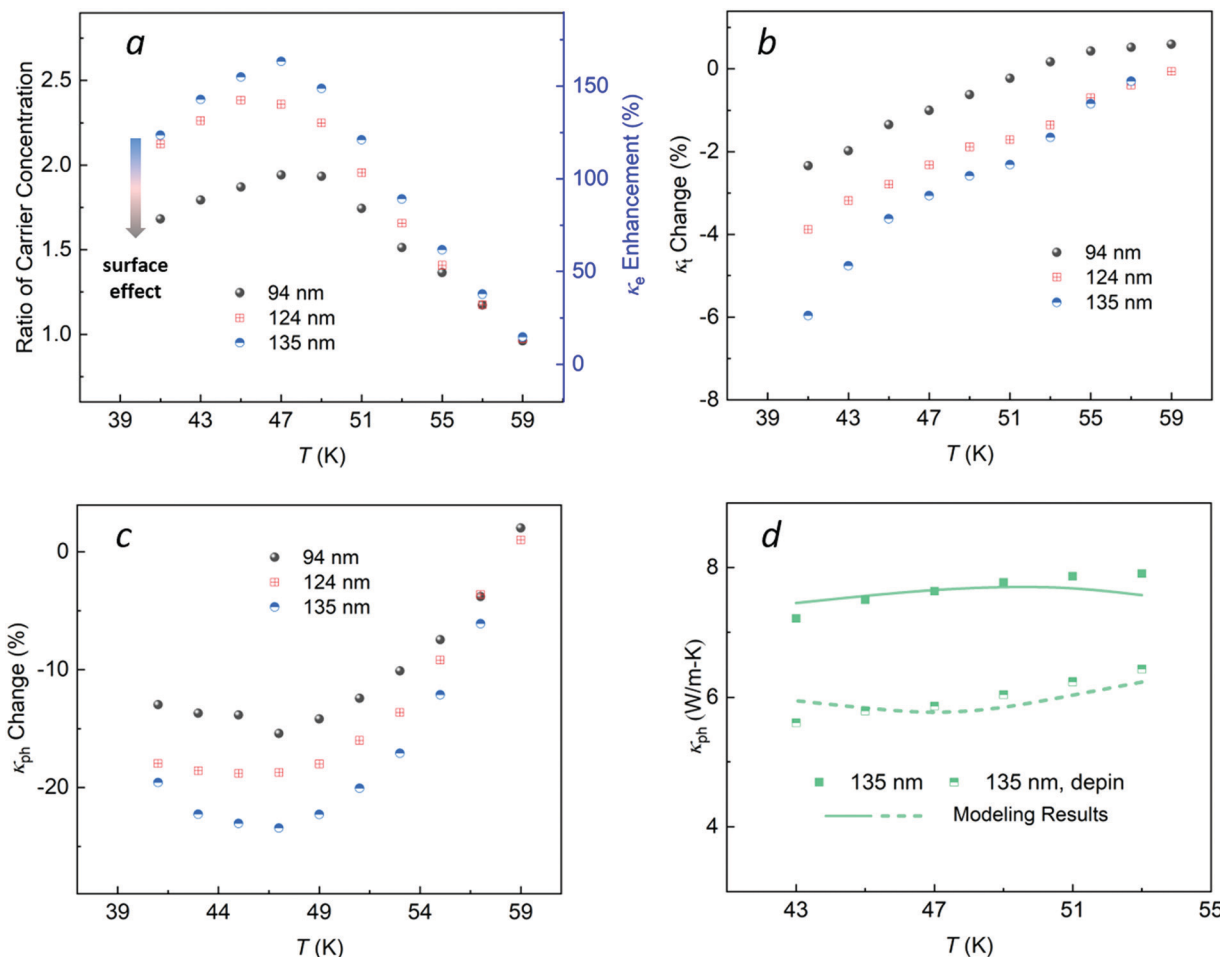


Fig. 3 Thermal properties upon depinning. (a) Carrier concentration variation (left axis) and corresponding electronic thermal conductivity enhancement (right axis). (b) Measured total thermal conductivity reduction. (c) Lattice thermal conductivity change. (d) Experimental results and first principles calculations of κ_{ph} ($D_h = 135$ nm).

not show enhancement in response to the increased κ_e upon depinning, but decreases as shown in Fig. 3b. The reduction in κ_t is more significant for thicker wires, corroborating with the higher r for larger wires. Depinning releases condensed free electrons, or it can be regarded as that CDW phase transition does not occur at 59 K. In this case, the distinct signatures in κ_{ph} and κ_e corresponding to the CDW disappear, as shown in Fig. 2a.

The lower κ_t indicates that the lattice contribution, κ_{ph} , decreases to a greater level than the enhancement in κ_e , as shown in Fig. 3c, which is due to the higher e-ph scattering rate as more free electrons are released. Based on the kinetic theory, the lattice thermal conductivity can be estimated as $\kappa_{ph} = \frac{1}{3}CvI$, where C , v , and I are the phonon heat capacity per unit volume, group velocity and mean free path (MFP), respectively. It has been reported that the heat capacity of NbSe_3 only changes by about 1% during the CDW phase transition at 59 K.⁴¹ In addition, recent inelastic X-ray scattering studies show no sign of softening in phonon dispersion,⁴² consistent with the observation of marginal change in the Young's modulus across

both CDW transitions.⁴³ These results indicate that the phonon group velocity remains approximately the same through the CDW phase transitions. As such, the reduction in κ_{ph} must come from the change in phonon MFP, primarily due to the enhanced e-ph scattering as electrons are depinned.

When measuring thermal transport under depinning conditions, an electric field is applied to the nanowire. While the effect of Joule heating from this electric field has been considered in the derivation of the nanowire thermal conductivity (Section I in the ESI†), one might question whether the electric field could influence thermal transport in other ways. First, the applied electric field will accelerate electrons, which may potentially affect the electronic thermal conductivity. However, the drift velocity is estimated to be < 0.02% of the Fermi velocity in NbSe_3 (Section III in the ESI†), which should not significantly affect the measured electronic thermal conductivity.

Another important factor when measuring the thermal conductance with a DC current through the nanowire sample is whether the Peltier effect alters the measured thermal conductivity. As discussed in the ESI,† we have carefully considered

the Peltier effect and show that it can be eliminated in the calculation. This is because our approach measures the relative temperature increases on both heating and sensing membranes when we apply Joule heating to the heating membrane. As such, both Joule heating and Peltier effect from the nanowire sample simply present a background signal that can be canceled out in the thermal conductance calculation. Recently, Dong *et al.*⁴⁴ suggested an electric field dependent thermal conductivity in ferroelectric P(VDF-TrFE) nanofibers. The electric field they used ($\sim 10^5 \text{ V cm}^{-1}$) is 5 order of magnitude higher than the value ($< 1.5 \text{ V cm}^{-1}$) in our depinning measurements, and the effect of the small electric field on κ_{ph} in our study should be negligible.

To further show that the change in κ_{ph} is due to e-ph scattering with released electrons, we modeled κ_{ph} through combined first-principles calculations and phenomenological model. The Vienna ab initio simulation package (VASP)⁴⁵ is used to derive the force constants with the same parameters as reported in our previous study.¹⁸ Then, the phonopy package⁴⁶ is used to determine the frequency and velocity of each phonon by calculating phonon dispersion of NbSe₃. Under the framework of the Boltzmann transport equation, κ_{ph} along the molecular chain direction can be calculated by

$$\kappa_{\text{ph}} = \frac{1}{k_B T \Omega N} \sum_j f_0(f_0 + 1) (\hbar \omega v_j)^2 \tau_j, \quad (1)$$

where k_B , T , Ω , N , \hbar , ω , v_j , f_0 and τ_j are Boltzmann constant, temperature, volume of unit cell, number of wave vector points, reduced Planck constant, phonon frequency, mode j -dependent phonon group velocity, Bose-Einstein distribution and mode j -dependent phonon relaxation time, respectively. Using Matthiessen's rule, τ_j is evaluated considering boundary scattering, Umklapp scattering, defects scattering and e-ph scattering, and these parameters are determined to be the same as those reported in literature.¹⁸ Here e-ph scattering is calculated using

$$\tau_{j,\text{e-ph}}^{-1} = \frac{(m_e E_D)^2 k_B T}{2\pi\rho\hbar^4 v_j^2} \chi_\omega, \quad (2)$$

where m_e , E_D and ρ denote the effective mass of electron, deformation potential and crystal mass density, and $\chi_\omega = \hbar\omega/k_B T$. The deformation potential depends on the carrier concentration according to $E_D = fn^{2/3}$, where F is a fitting parameter.⁴⁷ According to previous analysis, the depinning induced by the applied electric field will lead to an increase in the carrier concentration, resulting in an enhanced e-ph scattering rate. Thus, we can model κ_{ph} based on the electron concentration before and after depinning, and the calculation results (Fig. 3d) show that the model prediction fits the experimental data well. It is important to note that it has been suggested that the electron band shape does not change significantly upon depinning.⁴⁸ As such, the effective mass remains approximately the same with and without the depinning electric field. In fact, it has also been shown that the effective mass remains approximately the same across the CDW phase transition regime, further indicating that whether the charge carriers are free to move or pinned by defects and surface does not alter the

effective mass.⁴⁹ In fact, the effective mass is rather large, ~ 100 times the free electron mass,⁴⁹ as a result of strong e-ph coupling in NbSe₃.^{50,51}

The modelling results also show that comparing to other phonon scattering mechanisms, e-ph scattering indeed plays an important role in the relaxation time of phonons and it is the change in the e-ph scattering rate that leads to the reduced phonon MFP (Section IV in the ESI†). Moreover, the derived lattice thermal conductivity as a function of the depinning current for a 94 nm diameter wire at 47 K (Section V in the ESI†) indicates that the lattice thermal conductivity reduces as the depinning current escalates before it reaches 5.5 μA , beyond which no additional electrons are depinned. This observation suggests that the reduced lattice thermal conductivity is indeed due to the enhanced e-ph scattering as the free electron density increases upon depinning.

While the reduced κ_{ph} upon CDW depinning can be well-explained based on stronger e-ph scattering, in agreement with previous experiments,^{20,28} the overall reduction in κ_t is unexpected, which is different from the well-known plot illustrating the monotonically increasing trend of thermal conductivity as a function of the carrier concentration.¹ As the ratio of the carrier concentration change is less than 2.6 in our experiment, to explore the effects in a wider range, as shown in Fig. 4, we calculated the κ_{ph} for the 135 nm nanowire at 45 K with r increasing to 8. We also estimated κ_e using the Wiedemann-Franz law, and the relative change in κ_t is plotted on the right axis in Fig. 4. Indeed, for $r < 4.3$, the increase of κ_e cannot compensate for the reduction in κ_{ph} , which results in a net reduction in κ_t , consistent with our experimental data. However as r further increases, κ_{ph} gradually saturates and the enhancement in κ_e becomes more significant, which consequently leads to the increasing trend in κ_t .

It is important to note that the charge carrier concentration of the 135 nm NbSe₃ nanowire is estimated to be $3.5 \times 10^{19} \text{ cm}^{-3}$ at 45 K.

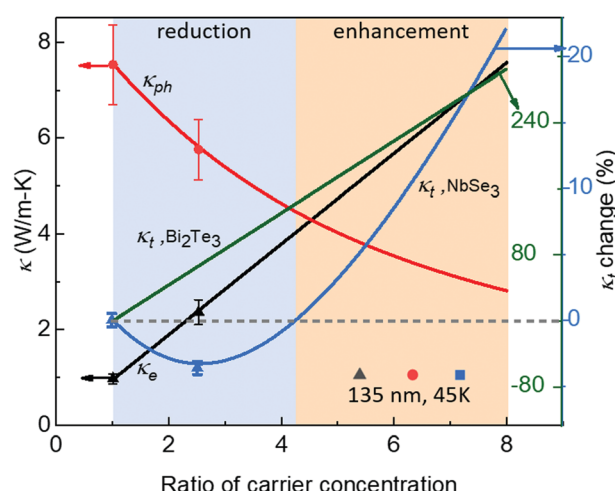


Fig. 4 Simulation results of thermal conductivity (κ_{ph} , κ_e , and κ_t) changes with carrier concentration ratio for $D_n = 135 \text{ nm}$ NbSe₃ nanowire at $T = 45 \text{ K}$. Dots in the plot are the experimental data showing good match with the simulation results. Data for Bi₂Te₃ is from literature.¹

At this relatively low electron concentration regime, the effects of e-ph scattering on κ_{ph} is not saturated, as shown in Fig. 4. Moreover, owing to the strong e-ph scattering among other scattering mechanisms in NbSe_3 ,¹⁸ the reduction of κ_{ph} caused by carrier concentration increase is larger than the κ_e increment, which explains a net negative change in κ_t . However, this could be different for other materials, for which even though κ_{ph} reduces as electron concentration increases, the relatively weak e-ph scattering would lead to a κ_{ph} reduction smaller than the κ_e enhancement. As shown in Fig. 4, we also plot the modeled relative κ_t change of Bi_2Te_3 in the same carrier concentration regime,¹ and different from our NbSe_3 nanowires, it exhibits a monotonically increasing trend as the charge carrier concentration increases.

Notably, unlike extrinsic doping, the unique advantage of depinning induced carrier concentration change in NbSe_3 nanowires is that it does not involve the effects from impurity scattering. Through careful comparison between the experimental data and modeling results, we exclusively show the lattice thermal conductivity reduction caused by e-ph scattering, and demonstrate a regime that is previously overlooked for

total thermal conductivity change as carrier concentration increases.

The change in κ_t upon depinning also provides a potential mechanism of tuning the materials thermal conductivity. While for NbSe_3 , the maximum tuning level is only $\sim 6\%$, similar mechanism of other CDW materials might provide a high on-off switch ratio. Control and modulation of material thermal properties is challenging but could impact a wide variety of applications and is being actively pursued by researchers.⁵² Different mechanisms have been explored to modulate thermal transport, such as asymmetric nanostructures,^{53–57} interface engineering,^{41–43,58} chemical composition modification,⁵⁹ magnetic or electric fields^{60,61} or structure modulation.^{62,63} Cartoixa *et al.*,⁵³ numerically studied thermal transport in telescopic Si nanowires. They observed a maximum thermal rectification of 50%. The modulation is achieved by the different temperature dependence for Si nanowires of different sizes. Ihlefeld *et al.*,⁶¹ claimed a maximum modulation in thermal conductivity of 11% with a giant electric field across nanoscale ferroelastic domain structure. Here we tested the modulation cycle using the depinning effect. A maximum modulation of $\sim 1.8 \text{ W} (\text{m K})^{-1}$ in κ_{ph} is achieved for the 135 nm sample, as shown in Fig. 5a. Repeated modulation in κ_t is confirmed in Fig. 5b as we switched the depinning voltage on and off. Collectively, our results demonstrate a new avenue to enable dynamic control of thermal transport in solid state systems through utilizing the CDW phase transition.

Summary

In summary, we conducted thermal conductivity measurements of NbSe_3 nanowires in the second CDW temperature regime without and with depinning electric field. Comparison of the results under these two conditions provides direct evidence of the competing effects of free electrons on thermal conductivity and discloses that free electrons could lead to a net negative contribution to the thermal conductivity of NbSe_3 . These data provide insights into the roles that free electrons plays in thermal transport and should have broad implications in thermal engineering.

Conflicts of interest

The authors declare no competing financial interest.

Acknowledgements

The authors thank the financial support from the U.S. National Science foundation (CBET-1805924 and DMR-1532107). Y. T. acknowledges financial support from the China Scholarship Council (CSC, 201806090027). This work was performed in part at Cornell NanoScale Facility, an NNCI member supported by NSF Grant NNCI-1542081. Support for crystal growth and characterization was provided by the National Science Foundation through the Penn State 2D Crystal Consortium-Materials Innovation Platform (2DCC-MIP) under NSF cooperative agreement

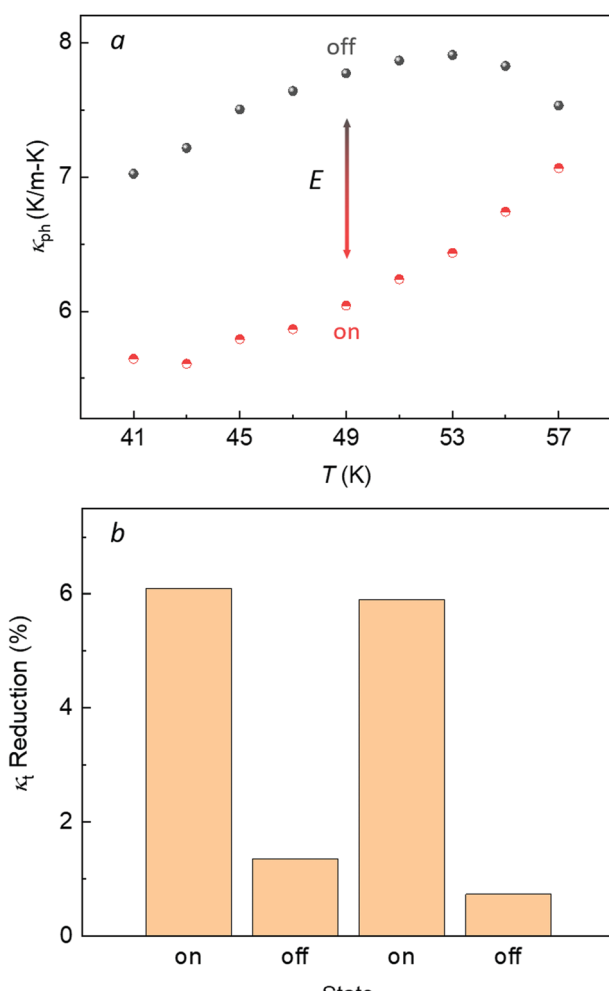


Fig. 5 Thermal switch behavior. (a) Measured lattice thermal conductivity variation during depinning test. ($D_h = 135 \text{ nm}$). (b) Repeatability demonstration ($D_h = 135 \text{ nm}$, $T = 41 \text{ K}$).

DMR-1539916. Z. Q. M. acknowledges the support of NSF-DMR-1917579.

Notes and references

- 1 G. Snyder and E. Toberer, *Nat. Mater.*, 2008, **7**, 105–114.
- 2 M. G. Holland, *Phys. Rev.*, 1964, **134**, A471–A480.
- 3 L. Lindsay, D. A. Broido and N. Mingo, *Phys. Rev. B: Condens. Matter Mater. Phys.*, 2010, **82**, 2–7.
- 4 J. S. Kang, M. Li, H. Wu, H. Nguyen and Y. Hu, *Science*, 2018, **361**, 575–578.
- 5 T. Feng, L. Lindsay and X. Ruan, *Phys. Rev. B*, 2017, **96**, 1–6.
- 6 D. Li, Y. Wu, P. Kim, L. Shi, P. Yang and A. Majumdar, *Appl. Phys. Lett.*, 2003, **83**, 2934–2936.
- 7 M. Asheghi, Y. K. Leung, S. S. Wong and K. E. Goodson, *Appl. Phys. Lett.*, 1997, **71**, 1798–1800.
- 8 W. Liu and M. Asheghi, *Appl. Phys. Lett.*, 2004, **84**, 3819–3821.
- 9 Y. S. Ju and K. E. Goodson, *Appl. Phys. Lett.*, 1999, **74**, 3005–3007.
- 10 C. T. Walker and R. O. Pohl, *Phys. Rev.*, 1963, **131**, 1433–1442.
- 11 J. H. Chen, W. G. Cullen, C. Jang, M. S. Fuhrer and E. D. Williams, *Phys. Rev. Lett.*, 2009, **102**, 1–4.
- 12 B. Liao, B. Qiu, J. Zhou, S. Huberman, K. Esfarjani and G. Chen, *Phys. Rev. Lett.*, 2015, **114**, 1–6.
- 13 Y. Wang, Z. Lu and X. Ruan, *J. Appl. Phys.*, 2016, **119**, 1–10.
- 14 A. Jain and A. J. H. McGaughey, *Phys. Rev. B*, 2016, **93**, 1–5.
- 15 Q. Xu, J. Zhou, T. H. Liu and G. Chen, *Appl. Phys. Lett.*, 2019, **115**, 1–4.
- 16 D. T. Morelli, J. P. Heremans, C. P. Beetz, W. S. Yoo and H. Matsunami, *Appl. Phys. Lett.*, 1993, **63**, 3143–3145.
- 17 B. Liao, A. A. Maznev, K. A. Nelson and G. Chen, *Nat. Commun.*, 2016, **7**, 1–7.
- 18 L. Yang, Y. Tao, J. Liu, C. Liu, Q. Zhang, M. Akter, Y. Zhao, T. T. Xu, Y. Xu, Z. Mao, Y. Chen and D. Li, *Nano Lett.*, 2019, **19**, 415–421.
- 19 H. Liu, C. Yang, B. Wei, L. Jin, A. Alatas, A. Said, S. Tongay, F. Yang, A. Javey, J. Hong and J. Wu, *Adv. Sci.*, 2020, **7**, 1–7.
- 20 R. M. Fleming, *Phys. Rev. B: Condens. Matter Mater. Phys.*, 1979, **19**, 3970–3980.
- 21 P. Monceau, N. P. Ong, A. M. Portis, A. Meerschaut and J. Rouxel, *Phys. Rev. Lett.*, 1976, **37**, 602–606.
- 22 G. Grüner, *Rev. Mod. Phys.*, 1988, **60**, 1129–1181.
- 23 L. Shi, D. Li, C. Yu, W. Jang, D. Kim, Z. Yao, P. Kim and A. Majumdar, *J. Heat Transfer*, 2003, **125**, 881–888.
- 24 M. C. Wingert, Z. C. Y. Chen, S. Kwon, J. Xiang and R. Chen, *Rev. Sci. Instrum.*, 2012, **83**, 1–7.
- 25 Q. Zhang, C. Liu, X. Liu, J. Liu, Z. Cui, Y. Zhang, L. Yang, Y. Zhao, T. T. Xu, Y. Chen, J. Wei, Z. Mao and D. Li, *ACS Nano*, 2018, **12**, 2634–2642.
- 26 L. Yang, Y. Yang, Q. Zhang, Y. Zhang, Y. Jiang, Z. Guan, M. Gerboth, J. Yang, Y. Chen, D. G. Walker, T. T. Xu and D. Li, *Nanoscale*, 2016, **8**, 17895–17901.
- 27 S. Onishi, M. Jamei and A. Zettl, *New J. Phys.*, 2017, **19**, 023001.
- 28 G. Grüner, A. Zawadowski and P. M. Chaikin, *Phys. Rev. Lett.*, 1981, **46**, 511–515.
- 29 N. P. Ong and P. Monceau, *Phys. Rev. B: Condens. Matter Mater. Phys.*, 1977, **16**, 3443–3455.
- 30 R. M. Fleming, D. E. Moncton and D. B. McWhan, *Phys. Rev. B: Condens. Matter Mater. Phys.*, 1978, **18**, 5560–5563.
- 31 J. Bardeen and W. Shockley, *Phys. Rev.*, 1950, **80**, 72–80.
- 32 X. D. Xiang and J. W. Bril, *Phys. Rev. B: Condens. Matter Mater. Phys.*, 1989, **39**, 1290–1297.
- 33 N. P. Ong, *Phys. Rev. B: Condens. Matter Mater. Phys.*, 1978, **18**, 5272–5279.
- 34 J. C. Gill, *EPL*, 1990, **11**, 175–180.
- 35 C. Brun, Z. Z. Wang and P. Monceau, *Phys. Rev. B: Condens. Matter Mater. Phys.*, 2009, **80**, 1–11.
- 36 S. Brazovskii, C. Brun, Z. Z. Wang and P. Monceau, *Phys. Rev. Lett.*, 2012, **108**, 1–4.
- 37 P. J. Yetman and J. C. Gill, *Solid State Commun.*, 1987, **62**, 201–206.
- 38 B. M. Murphy, J. Stettner, M. Traving, M. Sprung, I. Grotkopp, M. Müller, C. S. Oglesby, M. Tolan and W. Press, *Phys. B*, 2003, **336**, 103–108.
- 39 C. Brun, Z. Z. Wang, P. Monceau and S. Brazovskii, *Phys. Rev. Lett.*, 2010, **104**, 5–8.
- 40 S. V. Zaitsev-Zotov, V. Y. Pokrovskii and P. Monceau, *JETP Lett.*, 2001, **73**, 25–27.
- 41 S. Tomić, K. Biljaković, D. Djurek, J. R. Cooper, P. Monceau and A. Meerschaut, *Solid State Commun.*, 1981, **38**, 109–112.
- 42 H. Requardt, J. E. Lorenzo, P. Monceau, R. Currat and M. Krisch, *Phys. Rev. B: Condens. Matter Mater. Phys.*, 2002, **66**, 1–4.
- 43 J. W. Brill and N. P. Ong, *Solid State Commun.*, 1978, **25**, 1075–1078.
- 44 L. Dong, Q. Xi, J. Zhou, X. Xu and B. Li, *arXiv*, 2019.
- 45 G. Kresse and J. Furthmüller, *Comput. Mater. Sci.*, 1996, **6**, 15–50.
- 46 A. Togo, F. Oba and I. Tanaka, *Phys. Rev. B: Condens. Matter Mater. Phys.*, 2008, **78**, 1–9.
- 47 M. Asheghi, K. Kurabayashi, R. Kasnavi and K. E. Goodson, *J. Appl. Phys.*, 2002, **91**, 5079–5088.
- 48 J. P. Sorbier, H. Tortel, P. Monceau and F. Levy, *Phys. Rev. Lett.*, 1996, **76**, 676.
- 49 D. Reagor, S. Sridhar and G. Gruner, *Phys. Rev. B: Condens. Matter Mater. Phys.*, 1986, **34**, 2212.
- 50 J. L. Hodeau, M. Marezio, C. Roucau, R. Ayroles, A. Meerschaut, J. Rouxel and P. Monceau, *J. Phys. C*, 1978, **11**, 4134.
- 51 H. Requardt, J. E. Lorenzo, P. Monceau, R. Currat and M. Krisch, *Phys. Rev. B: Condens. Matter Mater. Phys.*, 2002, **66**, 214303.
- 52 S. Chu and A. Majumdar, *Nature*, 2012, **488**, 294–303.
- 53 X. Cartoixà, L. Colombo and R. Rurali, *Nano Lett.*, 2015, **15**, 8255–8259.
- 54 Y. Wang, A. Vallabhaneni, J. Hu, B. Qiu, Y. P. Chen and X. Ruan, *Nano Lett.*, 2014, **14**, 592–596.
- 55 C. W. Chang, D. Okawa, A. Majumdar and A. Zettl, *Science*, 2008, **314**, 1121–1124.

- 56 H. Wang, S. Hu, K. Takahashi, X. Zhang, H. Takamatsu and J. Chen, *Nat. Commun.*, 2017, **8**, 1–8.
- 57 J. Lee, V. Varshney, A. K. Roy, J. B. Ferguson and B. L. Farmer, *Nano Lett.*, 2012, **12**, 3491–3496.
- 58 J. Yang, Y. Yang, S. W. Waltermire, X. Wu, H. Zhang, T. Gutu, Y. Jiang, Y. Chen, A. A. Zinn, R. Prasher, T. T. Xu and D. Li, *Nat. Nanotechnol.*, 2012, **7**, 91–95.
- 59 J. Cho, M. D. Losego, H. G. Zhang, H. Kim, J. Zuo, I. Petrov, D. G. Cahill and P. V. Braun, *Nat. Commun.*, 2014, **5**, 2–7.
- 60 N. H. Thomas, M. C. Sherrrott, J. Brouillet, H. A. Atwater and A. J. Minnich, *Nano Lett.*, 2019, **19**, 3898–3904.
- 61 J. F. Ihlefeld, B. M. Foley, D. A. Scrymgeour, J. R. Michael, B. B. McKenzie, D. L. Medlin, M. Wallace, S. Trolier-McKinstry and P. E. Hopkins, *Nano Lett.*, 2015, **15**, 1791–1795.
- 62 A. J. H. Mante and J. Volger, *Physica*, 1971, **52**, 577–604.
- 63 J. Zhu, K. Hippalgaonkar, S. Shen, K. Wang, Y. Abate, S. Lee, J. Wu, X. Yin, A. Majumdar and X. Zhang, *Nano Lett.*, 2014, **14**, 4867–4872.